Multistage transformation and charge effect during the fragmentation phase transition in atomic clusters

D. Qian, X. Ma, Z. Chen, B. Li, X. Zhu, S. Zhang, Serge Martin, Richard Brédy, Jérôme Bernard, L. Chen

▶ **To cite this version:**

D. Qian, X. Ma, Z. Chen, B. Li, X. Zhu, et al.. Multistage transformation and charge effect during the fragmentation phase transition in atomic clusters. Physical Review A : Atomic, molecular, and optical physics [1990-2015], 2013, 87 (6), pp.063201. 10.1103/PhysRevA.87.063201 . hal-03146516

HAL Id: hal-03146516
https://hal.science/hal-03146516v1

Submitted on 19 Jan 2022

HAL is a multi-disciplinary open access archive for the deposit and dissemination of scientific research documents, whether they are published or not. The documents may come from teaching and research institutions in France or abroad, or from public or private research centers.

L'archive ouverte pluridisciplinaire **HAL**, est destinée au dépôt et à la diffusion de documents scientifiques de niveau recherche, publiés ou non, émanant des établissements d'enseignement et de recherche français ou étrangers, des laboratoires publics ou privés.

Multistage transformation and charge effect during the fragmentation phase transition in atomic clusters

D. B. Qian,[1] X. Ma,[1,*] Z. Chen,[1] B. Li,[1] X. L. Zhu,[1] S. F. Zhang,[1] S. Martin,[2] R. Brédy,[2] J. Bernard,[2] and L. Chen[2]

[1]*Institute of Modern Physics, Chinese Academy of Sciences, Lanzhou 730000, China*

[2]*Université de Lyon, F-69622, Lyon, France; Université Lyon 1, Villeurbanne; CNRS, UMR 5579, LASIM, France*

(Received 17 March 2013; published 25 June 2013)

Compared with the macrosystem case, the phase transition occurring in fragmenting cluster systems depicts a much richer story. However, most experimental observations have been restricted to an extremely partial view of this picture due to the technical limitations of a large-range scan of the energy deposited in a selected cluster system. Here, taking charge-selected $C_{60}{}^{3+}$ and $C_{60}{}^{4+}$ as model systems, we experimentally explore the fragmentation phase transition (FPT) over a large energy range and directly observe some of the most important features of the FPT, the multistage transformation, and the charge effect.

DOI: 10.1103/PhysRevA.87.063201 PACS number(s): 36.40.Ei, 36.40.Qv, 36.40.Wa

The fragmentation of finite systems such as hot clusters or hot nuclei, as an unconventional phase transition, has attracted increasing interest both experimentally [1–6] and theoretically [7–12]. Unlike the macrosystem case, theoretical treatment of the fragmentation phase transition (FPT) requires a microcanonical description. In a series of theoretical works from Gross's group [13–16], the calculated caloric curve for a cluster system was found to be divided into four parts: after an initially rising, a plateau and a backbending are present before the curve rises again. The results indicate a multistage FPT corresponding to a hierarchical opening of the cluster configuration with increasing energy, which was found also related to a stepwise appearance of typical fragmentation phenomena from no fragmentation (NF) through asymmetrical dissociation (AD) and multifragmentation (MF) to complete fragmentation (CF). Furthermore, the calculated FPT has significant dependence on the cluster size and the cluster charge. For example, charging the cluster shifts the transition to lower excitation energies and forces the transition region to narrow or even disappear [15]. These features were considered as signatures of charge effect on the FPT.

Since the notable work by Gross's group, several experiments have been performed in attempts to shed light on the FPT. Schmidt *et al.* [1] and Brechignac *et al.* [3] detected the FPT occurring in singly charged $Na_{139}{}^{+}$ and $Sr_n{}^{+}$ (n = 4–15) clusters by plotting the caloric curves over a limited energy range which is far from reaching the appearance of MF phenomena. Although the existence of FPT was demonstrated by their measurements, some important features of the FPT such as multistage transformation and charge effect are not observed. Actually, Gobet *et al.* [2] explored the FPT of $H_3{}^{+}(H_2)_m$ (m = 6–14) over a large energy range; nevertheless the accuracy of their observation was later questioned due to a controversial determination for the energy with the help of collision modeling [17].

The C_{60} molecule should be a good model system for studying FPT because experiments on C_{60} are much easier to perform than on other clusters. During the last decades, the fragmentation temperature of C_{60} has been determined theoretically to be about 6000 K with molecular dynamics simulations [18,19]. Recently, the Lyon's group developed a so-called collision-induced dissociation under energy control (CIDEC) technique [20,21] and achieved a large-range scan of the excitation energy E^* deposited in a charge-selected $C_{60}{}^{r+*}$. Despite detailed information about the fragmentation pattern obtained from the CIDEC experiment, the issue of FPT has not yet been explored even if a possible charge-assisted "phase change" was noticed in Ref. [21] by comparing the measured appearance energies of small fragments from MF of $C_{60}{}^{4+}$ with an early simulations for $C_{60}{}^{+}$ [22].

The conventional indicator of phase transition, based on the caloric curve, is not applicable to C_{60} because it is unlikely to measure the high temperature needed for the FPT under laboratory conditions. Here we propose the presence or absence of certain fragmentation phenomena as an indicator for characterizing the FPT. Based on such an indicator, we provide insight into the FPT occurring in cluster systems by reevaluating the data of charge-selected $C_{60}{}^{r+*}$ (r = 3, 4) published in Ref. [21]. The multistage transformation was obtained by showing the energy-dependent evolution of fragmentation phenomena. The charge effect was demonstrated by a comparison between the two systems with different initial charges.

The excited multiply charged $C_{60}{}^{r+*}$ (r = 3,4) parent ions were produced in collisions between a low-energy ion beam, F^{2+} at 6.8 keV, and a C_{60} jet via charge exchange. To apply the CIDEC method, events corresponding to the primary electron transfer processes

$$F^{2+} + C_{60} \rightarrow F^{-} + C_{60}^{r+*} + (r-3)\, e^{-}$$

were selected. The charge r of the parent ions prior to fragmentation was determined by detecting the number of ejected electron from thermal electronic ionization (TEI) in each collision, 0 e^- for $C_{60}{}^{3+*}$ and 1 e^- for $C_{60}{}^{4+*}$. The energy E_d deposited in the target during the collision was determined by measuring the kinetic energy loss ΔE of the scattered anion F^- and considering the energy defect of the reaction $\delta = -22.2$ eV. The simple energy balance relation $E_d = \Delta E - \delta$ used to convert the measured energy loss to the deposited energy was ensured by two conditions: the detected anion F^- was formed by the capture of three electrons directly

*x.ma@impcas.ac.cn

 ©2013 American Physical Society

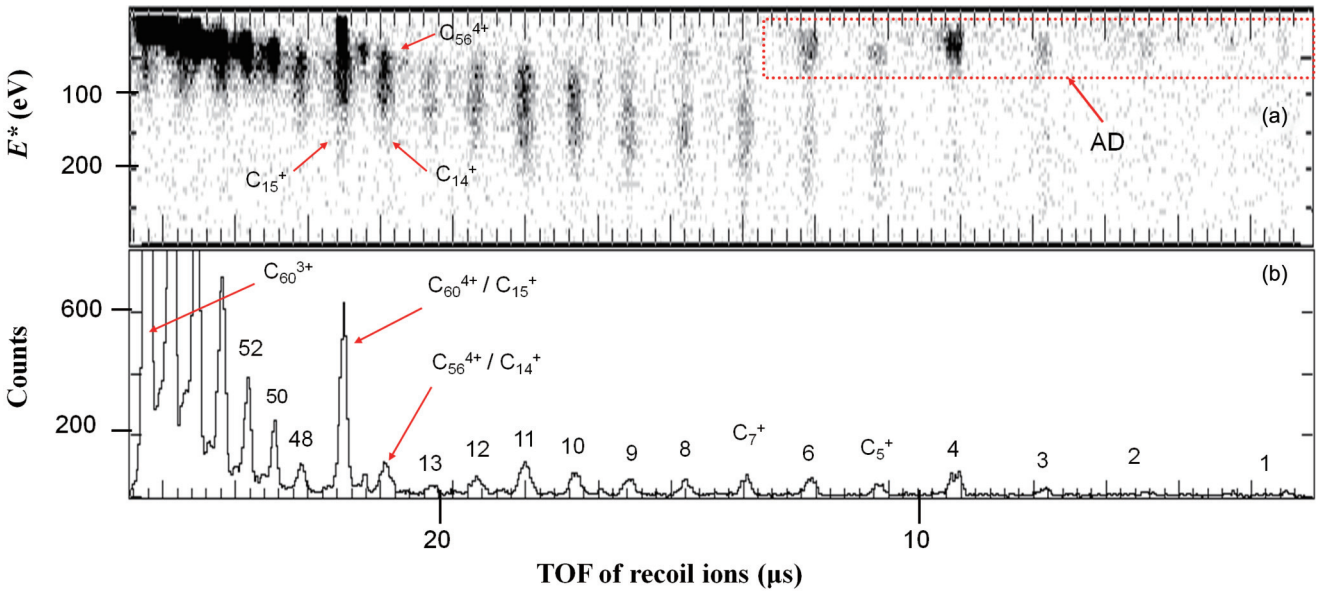

FIG. 1. (Color online) Spectra associated with the C_{60}^{3+*} parent ions. Spectrum (a) shows the correlation between excitation energy E^* and TOF of the heaviest recoil ions for each collision event. Based on such a correlation, the species and origin of recoil ions are unambiguously distinguished. Especially, the spots of mass over charge ratio $m/q = 14,15$ are distinguished as C_{56}^{4+}, C_{60}^{4+} in the lower energy region and as C_{14}^{+},C_{15}^{+} in the higher energy region; the spots of $m/q = 1$–6 are distinguished as originating from asymmetrical fission in the lower energy region outlined by a red square and from MF in the higher energy region. A small fraction of the spectrum belonging to C_{60}^{4+*} parent ions drops incidentally in this figure due to the limited electron detection efficiency. Spectrum (b) is obtained by projecting (a) onto the TOF axis.

to the ground state and the recoil kinetic energy of the target was negligible. The time of flight (TOF) of the recoil ions, the kinetic energy loss of F^-, and the number of ejected electrons were measured in an event-by-event mode. The E^* of C_{60}^{3+*} prior to fragmentation was obtained from E_d by adding 5 eV, the initial excitation energy of C_{60} due to the temperature of the oven heated to 500 °C. For the case of C_{60}^{4+}, assuming that the kinetic energy of the TEI electron was negligible, the E^* of C_{60}^{4+} was obtained from E_d by adding 5eV and then removing the fourth ionization potential ($IP_4 = 17.8$ eV) of C_{60}.

Figure 1 shows that the triply charged parent ions C_{60}^{3+*} dissociate mainly by the evaporation of C_2 units leading to the dominant triply charged fullerene peaks (C_{60-2n}^{3+}, $n = 1$–6). Minor doubly charged fullerene peaks (C_{60-2n}^{2+}) originating from asymmetrical fission are not shown in the figure; instead, the correlated small charged fragments, plotted due to the limited ion detection efficiency, can be seen in the region enclosed by the red dotted-line square. In the case of C_{60}^{4+*}, both quadruply (C_{58}^{4+} and C_{56}^{4+}) and triply (C_{60-2n}^{3+}, $n = 1$–6) charged fullerene ions are observed in the spectra (Fig. 2). The above fragmentation channels characterized by the existence of a large fullerene fragment represent AD phenomena. The stable parent ions correspond to the NF phenomena. All smaller fragments (C_n^+ and C_n^{2+}, $n = 1$–23) for both C_{60}^{3+*} and C_{60}^{4+*} represent MF phenomena except for those related to asymmetrical fission.

Taking C_{60}^{4+*} parent ions as an example, in Figs. 2(b-1) to 2(b-4) we present four differential TOF spectra over an energy interval of 20 eV. From the fragment distributions in the spectra, one could observe the evolution of fragmentation phenomena from NF to AD and to MF with increasing energy. To get precise characterization for the evolution, we intend to quantitatively provide the population distribution of fragmentation phenomena over a narrower energy interval. Here, the differential TOF spectra were first obtained by the projection of the two-dimensional spectrum [Fig. 2(a)] over energy intervals of 5 eV, and then each differential spectrum was corrected from event loss due to the limited ion detection efficiency (80%) and from mutual contamination due to the limited electron detection efficiency (75%). From each modified spectrum, the population distribution of each phenomenon was obtained by accumulating the event counts of NF phenomena (N_{NF}), AD phenomena (N_{AD}), and MF phenomena (N_{MF}) with E^* sampled equidistantly up to 210 eV.

In Fig. 3 we have plotted the population distributions of fragmentation phenomena associated with C_{60}^{4+*}as a function of E^* and find obvious twofold coexistence of the NF and AD phenomena in the low E^* region and of the AD and MF phenomena in the high E^* region. From these evolution curves, four characteristic energy points should be noticed: the first appearance of AD phenomena and the first disappearance of NF phenomena denoting respectively the lower and upper limits of the NF-AD coexistence region, and the first appearance of MF phenomena and the first disappearance AD phenomena denoting respectively the lower and upper limits of the AD-MF coexistence region. To obtain an accurate determination for these characteristic points and a visual description for the multiphenomena transformation, we define two ratio parameters Γ_{NF} and Γ_{AD}, where Γ_{NF} is the ratio of NF population over the sum of NF and AD populations,

$$\Gamma_{NF} = \frac{N_{NF}}{N_{NF} + N_{AD}}, \quad (1)$$

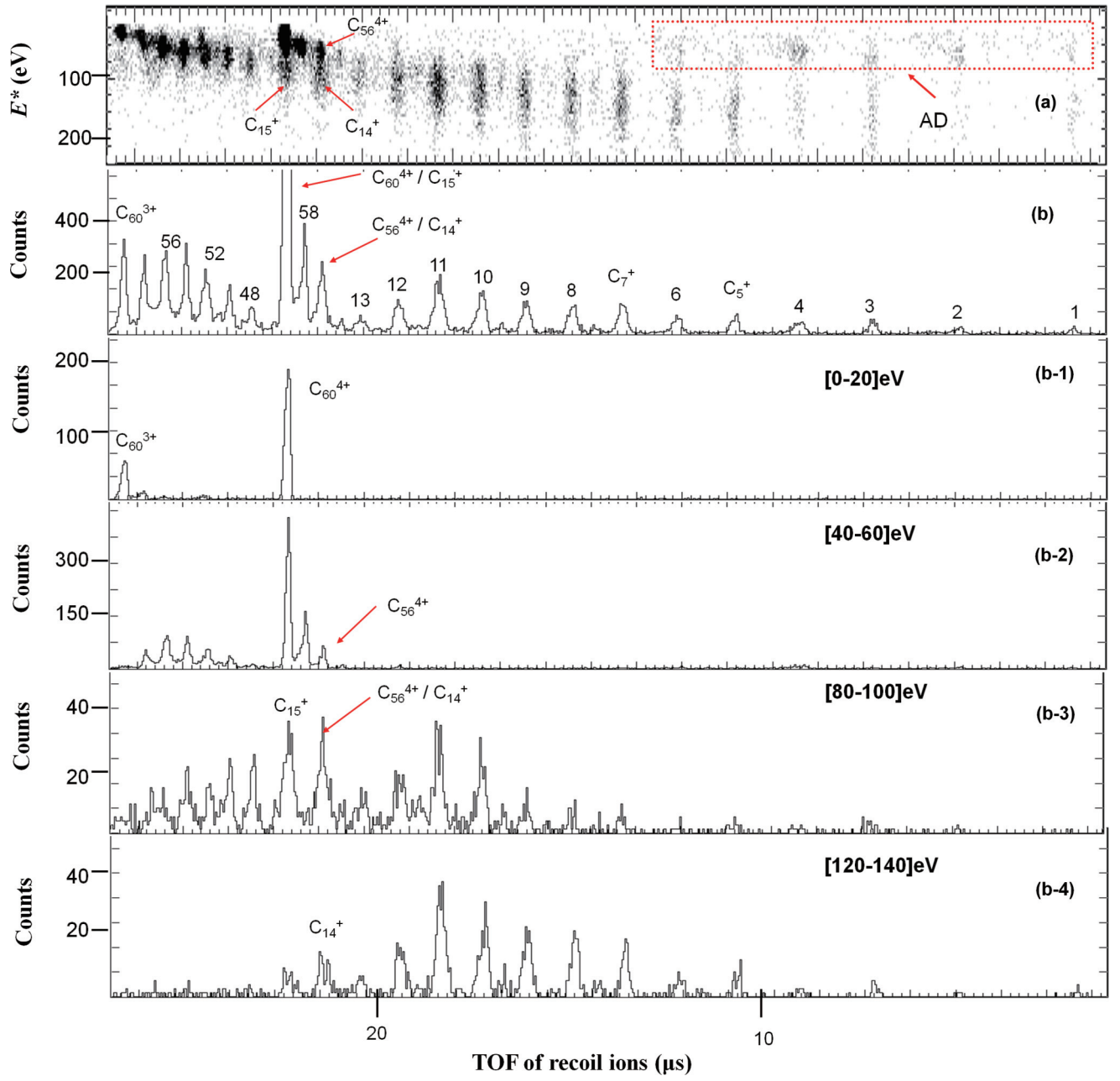

FIG. 2. (Color online) Spectra associated with the C_{60}^{4+*} parent ions. For spectra (a) and (b), the notes are similar to Fig. 1. Minor differences are that a small fraction of spectrum belonging to C_{60}^{3+*} parent ions drops incidentally in this figure due to the noise of the electron detector. Differential spectra (b-1) to (b-4) are obtained by projecting (a) onto the TOF axis in four selected E^* regions: (b-1), nearly pure NF phenomena; (b-2), coexistence of NF and AD phenomena; (b-3), coexistence of AD and MF phenomena; (b-4), nearly pure MF phenomena.

and Γ_{AD} is the ratio of AD population over the sum of AD and MF populations,

$$\Gamma_{AD} = \frac{N_{AD}}{N_{AD} + N_{MF}}. \quad (2)$$

The Γ_{NF} and Γ_{AD} ratios as functions of E^* are displayed in Fig. 4. In the case of the $\Gamma_{AD}(E^*)$ curve, for $E^* < 55$ eV, Γ_{AD} is around 1 and the AD is the dominating fragmentation phenomena. For $E^* > 109$ eV, Γ_{AD} tends asymptotically to zero and the MF phenomena become predominant. A steep linear dropdown of Γ_{AD} is observed within the range of $55 \pm 3 < E^* < 109 \pm 3$ eV, corresponding to the transformation from AD to MF. The $\Gamma_{NF}(E^*)$ curve presents similar features with the steep linear dropdown observed for $31 \pm 3 < E^* < 58 \pm 3$ eV. For both curves, the fast linear decrease was observed within well-defined phenomena coexistence regions. It provides actually a signature for the two-stage transformation. The measured characteristic energy points are remarkable. Typically, the upper limits of the NF-AD stage and the lower limits of the AD-MF stage are found to be 58 ± 3 and 55 ± 3 eV, respectively, indicating the absence of a threefold coexistence. The behavior is in qualitative agreement with the typical features of the FPT predicted by Gross's group [13–16]. Actually, the experimental observations of the

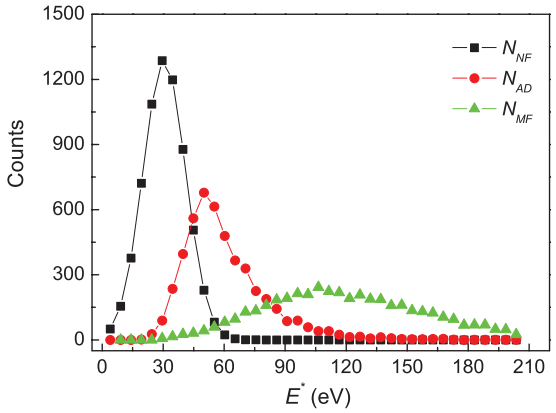

FIG. 3. (Color online) Population distributions of fragmentation phenomena associated with C_{60}^{4+*} parent ions as a function of E^*.

multistage transformation is similar to that of the melting phase transition occurring in an atomic cluster, which was proved continually to be a multistage process initiated by a "premelting" stage where the surface of a cluster melts before the core [23,24]. Both multistage processes are related to a hierarchical opening of the configuration space of cluster systems with E^* increasing. From the width of transition region for each stage (see Fig. 4), the apparent heat of transition was deduced to be about 0.45 eV/atom for the NF-AD stage and 0.9 eV/atom for the AD-MF stage. For comparison, the total apparent heat (1.35 eV/atom) corresponding to the two stages is dramatically smaller than the vaporization heat (7.4 eV/atom) of bulk graphite [25]. The large difference is not surprising because, although this work studies the FPT over a large energy range, the stage of transformation from MF to CF phenomena in much higher energy region is not reached.

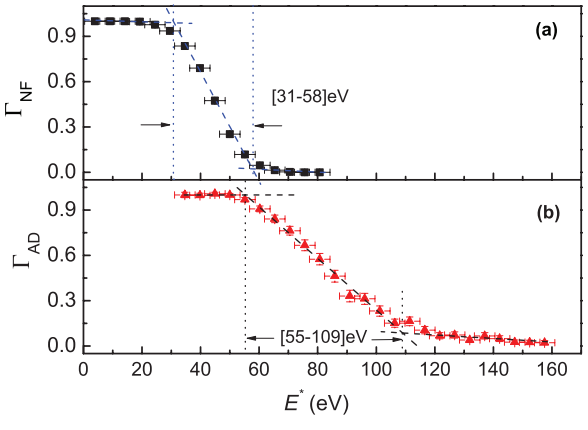

FIG. 4. (Color online) Population ratio of fragmentation phenomena associated with C_{60}^{4+*} parent ions as a function of E^*. (a) the Γ_{NF} (E^*) curve, and (b) the Γ_{AD} (E^*). The error bars of the ratio parameters are the statistical deviation, and the error bars of energy represent 1σ standard deviation of the instrumental broadening. Each curve can be divided into three linear regions with different slopes, and the dashed lines plotted in each region are linear fits by weighted least-squares method. Each intersection of two fitting lines represents a characteristic energy point (see the text). The dotted lines indicate the positions of the turning points.

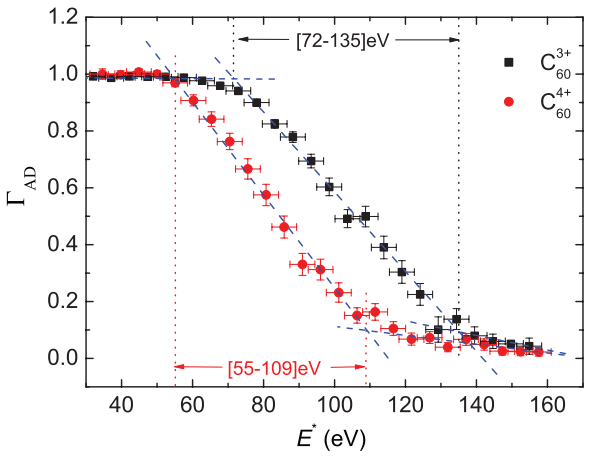

FIG. 5. (Color online) Γ_{AD} ratios associated with C_{60}^{r+*} (r = 3,4) parent ions as a function of E^*. The notes for the error bars and the fit are the same as in Fig. 4.

To illustrate the charge effect, in Fig. 5 we display together the Γ_{AD} for parent ions C_{60}^{3+*} and C_{60}^{4+*} as a function of E^*. Similar to C_{60}^{4+} case, the $\Gamma_{AD}(E^*)$ curve for C_{60}^{3+*} also has a transition region from 72 $\pm$ 3 to 135 $\pm$ 3 eV. In a comparison of the two curves, the width of the transition region associated with C_{60}^{4+*} has a noticed reduction of about 9 eV, suggesting a charge-induced reduction or suppression of the region. Similar charge behavior has been predicted for the FPT of nuclei [10] and of atomic clusters [15]. Such a behavior, in the simulation of nuclei cases, was attributed to a deformation of the event probability distributions and a rotation of the order parameter due to the repulsive Coulomb interaction. Another noteworthy feature shown in Fig. 5 is the shift of the transition region for C_{60}^{4+} compared to C_{60}^{3+}. The lower limit of this region is defined as the onset energy of the transition. Typically, the onset energy is found to be 55 and 72 eV for C_{60}^{4+} and C_{60}^{3+}, respectively, showing a significant shift of about 17 eV to lower E^* for C_{60}^{4+}. This variation tendency also shows the important role of the charge effect on the FPT. In fact, for a multiply charged system, the electrostatic potential energy should be considered as a part of the total energy available for the fragmentation. Therefore, the higher the charge, the lower the E^* required for driving the occurrence of FPT.

Especially deserved to be mentioned is the fact that the quantitative description of FPT depends sensitively on the excitation and ionization mechanism and the observation time window. In the recent theoretical investigation on charge-dependent FPT of C_{60}^{r+} (r = 0–24) [8], the mean fragment size $\langle n \rangle$ from the fragmentation of an ensemble of C_{60}^{r+} parent ions was presented as a function of E^* and a weak charge effect was observed [26]. In our experiments, the multielectron transfer happened in near C_{60} surface collisions. The sudden loss of three or four electrons during the collision in less than 1 fs led to the fast excitation and ionization of the C_{60} target. However, the theoretical work employed a ramp-like input of both excitation energy and charge with a ramp duration of 0.1 ps. Without a doubt, such a slow charge input process would result in a noticeable weakening of the charge effect. Furthermore, the experimental observation time scale is about 1 μs, while the theoretical observation time is about 2 ps. Recently, Calvo [9]

calculated the time-dependent FPT based on a kinetic Monte Carlo method, and predicted that increasing the observation time can shift the onset energy of transition to a lower energy region. It implies that the observation time window must also be taken into consideration when quantitatively describing the FPT.

In summary, from the experimental side, we provide clear evidence for the multistage transformation and charge effect during the FPT in atomic clusters. Furthermore, this study shows that the presence or absence of certain fragmentation phenomena can be used as an indicator to mark the FPT when the system temperature cannot be determined in experiments. To get a better understanding on the multistage process and the charge effect, experiments on the FPT with broader energy and charge ranges as well as theoretical investigations using simulation conditions close to the experiment settings would be anticipated. In the future, the indicator of phase transition presented in this paper may be extended to the experimental study of FPT occurring in other isolated systems such as complex molecules and nuclei.

This work was partly supported by the '973' Program (No. 2010CB832902), the NSFC (No. U1232122, 10904152), and the CNRS of France (PICS n°5722).

[1] M. Schmidt, T. Hippler, J. Donges, W. Kronmuller, B. von Issendorff, H. Haberland, and P. Labastie, Phys. Rev. Lett. **87**, 203402 (2001).
[2] F. Gobet, B. Farizon, M. Farizon, M. J. Gaillard, J. P. Buchet, M. Carre, and T. D. Mark, Phys. Rev. Lett. **87**, 203401 (2001); F. Gobet, B. Farizon, M. Farizon, M. J. Gaillard, J. P. Buchet, M. Carre, P. Scheier, and T. D. Mark, *ibid.* **89**, 183403 (2002).
[3] C. Brechignac, P. Cahuzac, B. Concina, and J. Leygnier, Phys. Rev. Lett. **89**, 203401 (2002).
[4] M. D'Agostno *et al.*, Nucl. Phys. A **650**, 329 (1999); Phys. Lett. B **473**, 219 (2000).
[5] J. Pochodzalla *et al.*, Phys. Rev. Lett. **75**, 1040 (1995).
[6] E. Bonnet *et al.*, Phys. Rev. Lett. **103**, 072701 (2009).
[7] D. H. E. Gross, Phys. Rep. **279**, 119 (1997).
[8] T. A. Beu, L. Horvath, and I. Ghisoiu, Phys. Rev. B **79**, 054112 (2009); T. A. Beu and A. Jurjiu, *ibid.* **83**, 024103 (2011).
[9] F. Calvo, Phys. Rev. A **71**, 041201 (2005).
[10] F. Gulminelli, P. Chomaz, A. H. Raduta, and A. R. Raduta, Phys. Rev. Lett. **91**, 202701 (2003).
[11] Ph. Chomaz, V. Duflot, and F. Gulminelli, Phys. Rev. Lett. **85**, 3587 (2000).
[12] L. G. Sobotka, R. J. Charity, J. Toke, and W. U. Schroder, Phys. Rev. Lett. **93**, 132702 (2004).
[13] D. H. E. Gross, M. E. Madjet, and O. Schapiro, Z. Phys. D **39**, 75 (1997).
[14] M. E. Madjet, P. A. Hervieux, D. H. E. Gross, and O. Schapiro, Z. Phys. D **39**, 309 (1997).
[15] O. Schapiro, P. J. Kuntz, K. Möhring, P. A. Hervieux, D. H. E. Gross, and M. E. Madjet, Z. Phys. D **41**, 219 (1997).
[16] D. H. E. Gross and M. E. Madjet, Z. Phys. B **104**, 541 (1997).
[17] M. Chabot and K. Wohrer, Phys. Rev. Lett. **93**, 039301 (2004).
[18] S. G. Kim and D. Tomanek, Phys. Rev. Lett. **72**, 2418 (1994).
[19] L. Horváth and T. A. Beu, Phys. Rev. B **77**, 075102 (2008).
[20] L. Chen, S. Martin, J. Bernard, and R. Bredy, Phys. Rev. Lett. **98**, 193401 (2007).
[21] S. Martin, L. Chen, A. Salmoun, B. Li, J. Bernard, and R. Bredy, Phys. Rev. A **77**, 043201 (2008).
[22] E. E. B. Campbell, T. Raz, and R. D. Levine, Chem. Phys. Lett. **253**, 261 (1996).
[23] G. A. Breaux, C. M. Neal, B. Cao, and M. F. Jarrold, Phys. Rev. Lett. **94**, 173401 (2005).
[24] C. Hock, C. Bartels, S. Strassburg, M. Schmidt, H. Haberland, B. von Issendorff, and A. Aguado, Phys. Rev. Lett. **102**, 043401 (2009).
[25] http://www.chemicool.com/elements/carbon.html.
[26] Titus Adrian Beu (private communication).